Letter

Emergence of charge loop current in the geometrically frustrated Hubbard model: A functional renormalization group study

Rina Tazai, Youichi Yamakawa, and Hiroshi Kontani
Department of Physics, Nagoya University, Furo-cho, Nagoya 464-8602, Japan

(Received 16 October 2020; revised 26 February 2021; accepted 6 April 2021; published 28 April 2021)

Spontaneous current orders due to odd-parity order parameters have attracted increasing attention in various strongly correlated metals. we discover a spin-fluctuation-driven charge loop current (cLC) mechanism based on the functional renormalization group theory. The present mechanism leads to the ferro-cLC order in a simple frustrated chain Hubbard model. The cLC appears between the antiferromagnetic and d-wave superconducting (dSC) phases. While the microscopic origin of the cLC has a close similarity to that of the dSC, the cLC transition temperature T_{cLC} can be higher than the dSC one for a wide parameter range. Furthermore, we reveal that the ferro-cLC order is driven by the strong enhancement of the forward scatterings g_2 and g_4 owing to the two dimensionality based on the g-ology language. The present study indicates that the cLC can emerge in metals near the magnetic criticality with geometrical frustration.

DOI: 10.1103/PhysRevB.103.L161112

Various exotic symmetry-breaking phenomena are recent central issues in strongly correlated metals. For instance, the violation of rotational symmetry, the so-called nematic order, has been intensively studied in Fe-based [1–7] and cuprate [8–17] superconductors in addition to heavy fermion compounds [18,19]. Many kinds of even-parity and time-reversal invariant unconventional orders, such as the orbital order [5–7], the d-wave bond order [8–16], and the spin-nematic order [1–4], have been proposed as candidates for the nematic order. (Bond order is the symmetry breaking in correlated hopping integrals.) Although the microscopic mechanism of the nematicity is still under debate, it is believed that many-body effects beyond the mean-field theory are significant [1–19].

When unconventional order violates the parity and/or time-reversal symmetries, more exotic phenomena emerge. For example, parity-violating bond order induces a spontaneous spin current [20,21]. Also, time-reversal violating order causes a static charge current, which accompanies the internal magnetic field that is measurable experimentally. Various charge loop currents (cLCs), such as the intraunit cell cLC [22,23] and antiferro-cLC [24–30], have been discussed. In square lattice models, the cLC due to nonzero spin chirality has been studied based on SU(2) gauge theory [31,32]. In addition to that, the generalized Hubbard ladder system has been studied by functional renormalization group and bosonization [33,34].

Recently, some experimental evidence for the cLC order has been reported. For instance, in quasi-one-dimensional (1D) two-leg ladder cuprates, polarized neutron diffraction (PND) reveals broken time-reversal symmetry [35] and concludes that the cLC appears. The cLCs are also reported in cuprates [36,37] and iridates [38] by PND studies, and their existence is supported by optical second harmonic generation (SHG) [39,40], Kerr effect [41], and magnetic torque [42] measurements.

These observations indicate the existence of a universal mechanism of the cLC that is closely related to the magnetic criticality. However, its microscopic origin is still unknown. Based on a simple Hubbard model with an on-site Coulomb interaction U, mean-field theories fail to explain the cLC. Therefore, off-site Coulomb and Heisenberg interactions have been analyzed [20,25]. However, the off-site bare interaction is much smaller than U in the usual metals. Then, we encounter the following essential questions: What is the minimum model to understand the cLC? What is the relation between cLC and magnetic criticality?

In this Letter, we propose a spin-fluctuation-driven cLC mechanism based on the functional renormalization group (fRG) theory [43–52]. Here, we optimize the form factor, which characterizes the essence of the unconventional order, unbiasedly based on the Lagrange multiplier method. By virtue of this method, the ferro-cLC order is obtained without bias in a simple frustrated chain Hubbard model given in Fig. 1(a). We discover that the cLC appears between the antiferromagnetic (AFM) phase and d-wave superconducting (dSC) phase as schematically shown in Fig. 1(b). The present theory indicates that cLC can emerge in strongly correlated electron systems with geometrical frustration.

The dimensional crossover in the coupled chain model has been studied intensively for years [53–58]. For $T \gg t^{\perp}$, each Hubbard chain is essentially independent because the thermal de Broglie wavelength is extremely short. For $T \ll t^{\perp}$, interchain coherence is established, and therefore a quasi-two-dimensional Fermi liquid (FL) state with a finite quasiparticle weight is realized. In the latter case, the one-loop fRG method is very useful since the incommensurate nesting vector of the Fermi surface (FS) is accurately incorporated into the theory. In g-ology language [53–59], the cLC order in the present theory is caused by the strong renormalization of the forward scatterings g_2 and g_4 owing to the two dimensionality.

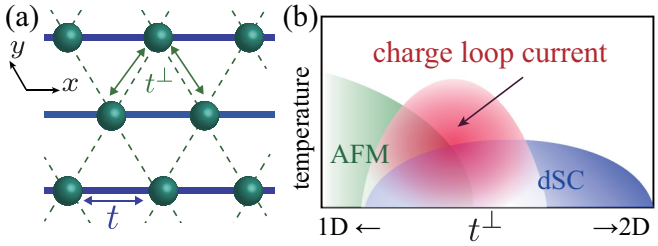

FIG. 1. (a) Lattice structure with intra- (t) and inter- ($t^\perp$) chain hoppings. (b) Schematic phase diagram. The cLC phase appears between the AFM and dSC phase.

Here, we study quasi-one-dimensional (Q1D) electron systems described by $\hat{H} = \hat{H}_0 + \hat{H}'$. The kinetic term is $\hat{H}_0 = \sum_{\boldsymbol{k}\sigma} \epsilon_{\boldsymbol{k}} c^\dagger_{\boldsymbol{k}\sigma} c_{\boldsymbol{k}\sigma}$, where $c^\dagger$ is a creation operator for the electron with the momentum $\boldsymbol{k}$ and spin σ. The energy dispersion is simply given by $\epsilon_{\boldsymbol{k}} = -2t\cos k_x - 2t^\perp\{\cos k_y + \cos(k_x + k_y)\} - \mu$ with $t = 1$ and the chemical potential μ. The inter-chain hopping $t^\perp$ ($\ll 1$) controls the dimensionality; $t^\perp \to 0$ corresponds to a complete 1D system. We also introduce an on-site Coulomb interaction $\hat{H}' = \sum_i U n_{i\uparrow} n_{i\downarrow}$ where i is the site index.

Now, we perform the fRG method to derive an effective low-energy interaction. In the present numerical study, we divide each left-Brillouin zone (BZ) and right-BZ into 24 patches. The center points of the patches $\boldsymbol{p}_i$ are shown in Fig. 2(a) and the Supplemental Material A (SM A) [60]. Here, we introduce a logarithmic energy scaling parameter $\Lambda_l = \Lambda_0 e^{-l}$ ($0 \leqslant l \leqslant l_c$) for $\Lambda_0 = 3$, which is slightly larger than $\max_{\boldsymbol{k}} |\epsilon_{\boldsymbol{k}}| \simeq 2.8$. In the following numerical study, we consider the half-filling case and put $l_c = 8.7$ ($\Lambda_{l_c} = T/100$) and $U = 2.01$ in the unit $t = 1$. Also, we fix $(t^\perp, T) = (0.2, 0.05)$ except for the phase diagram in Fig. 3. During the fRG analysis, the low-energy effective interaction changes with the cutoff Λ_l. It is represented on the patches as

$$\hat{H}'_{\rm eff} = \frac{1}{4}\sum_{\{p_i\}} g_{p_1p_2p_3p_4} c^\dagger_{p_1} c_{p_2} c_{p_3} c^\dagger_{p_4}, \tag{1}$$

where $\hat{g}$ is antisymmetric four-point vertex function with patch $\boldsymbol{p}_i$ and spin index where $p_i \equiv (\boldsymbol{p}_i, \sigma_i)$. $\hat{g}$ is defined in Fig. 2(b), and its initial condition is $g_{p_1p_2p_3p_4} = U\delta_{\boldsymbol{p}_1+\boldsymbol{p}_4,\boldsymbol{p}_2+\boldsymbol{p}_3}(\delta_{\sigma_1,\sigma_3}\delta_{\sigma_2,\sigma_4} - \delta_{\sigma_1,\sigma_2}\delta_{\sigma_3,\sigma_4})$. Then, $\hat{g}$ is calculated by solving the one-loop RG equation,

$$\frac{d}{d\Lambda_l} g_{p_1p_2p_3p_4} = \sum_{pp'}\left[\frac{1}{2}\frac{dW^-_{p,p'}}{d\Lambda_l} g_{p_1pp'p_4} g_{pp_2p_3p'} + \frac{dW^+_{p,p'}}{d\Lambda_l}\left(g_{p_1p_3pp'} g_{pp'p_2p_4} - g_{p_1p_2pp'} g_{pp'p_3p_4}\right)\right], \tag{2}$$

where $W^\pm_{p,p'} = T\sum_{\boldsymbol{k}\boldsymbol{k}'n} G_{\boldsymbol{k}n} G_{\boldsymbol{k}'\pm n} \Omega_{\boldsymbol{p}}(\boldsymbol{k})\Omega_{\boldsymbol{p}'}(\boldsymbol{k}')$. Here, $G_{\boldsymbol{k}n} \equiv (i\epsilon_n - \epsilon_{\boldsymbol{k}})^{-1}\theta(\Lambda_l - |\epsilon_{\boldsymbol{k}}|)$, and $\Omega_{\boldsymbol{p}}(\boldsymbol{k}) = 1$ (0) only if the momentum $\boldsymbol{k}$ is inside (outside) the $\boldsymbol{p}$ patch. Here, ϵ_n is the fermion Matsubara frequency. The first term on the right-hand side of Eq. (2) is the particle-particle loop [=Cooper-channel (ch)], and the second and third terms are the particle-hole loops (=Peierls-ch). Their diagrammatic expressions are given in SM A [60].

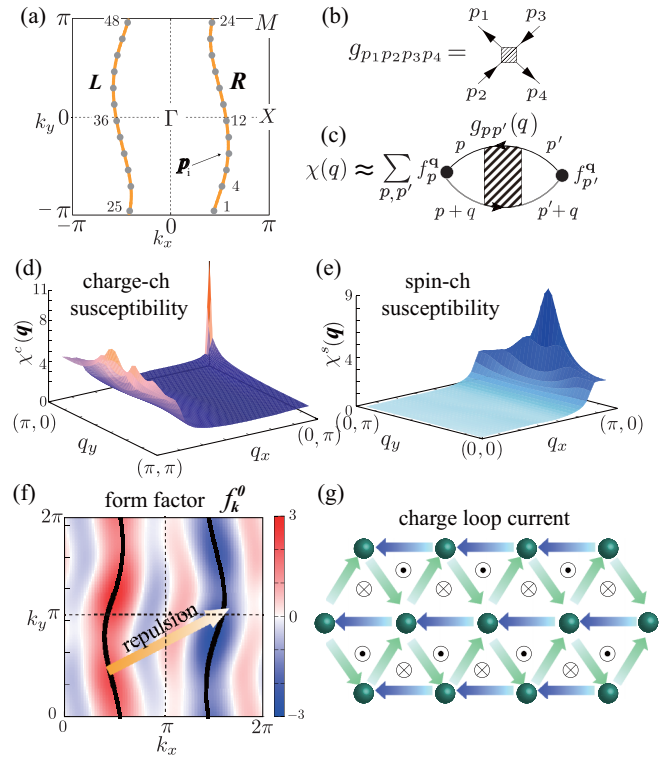

FIG. 2. (a) FS with center positions of the patches. (b) Four-point vertex function $\hat{g}$. (c) Susceptibility with the form factor $f^{\boldsymbol{q}}_{\boldsymbol{p}}$. (d) Development of $\chi^c(\boldsymbol{q})$ at $\boldsymbol{q} = \boldsymbol{0}$, which leads to the ferro-cLC. (e) Spin susceptibility with the peak at $\boldsymbol{q} = (\pi, \pi/2)$. (f) Obtained charge-channel form factor $f^{\boldsymbol{q}=\boldsymbol{0}}_{\boldsymbol{k}}$ ($\propto \sin k_x + b \sin 3k_x$). (g) Schematic picture of the cLC.

Here, we calculate the particle-hole susceptibilities, which are essentially given by the four-point vertex function in Fig. 2(c). The static charge (spin)-ch susceptibilities with the form factor $f^{\boldsymbol{q}}_{\boldsymbol{k}}$ are defined by

$$\chi^{c(s)}(\boldsymbol{q}) = \int_0^{T^{-1}} d\tau \frac{1}{2}\langle A^{c(s)}(\boldsymbol{q},\tau) A^{c(s)}(-\boldsymbol{q},0)\rangle,$$
$$A^{c(s)}(\boldsymbol{q},\tau) \equiv \sum_{\boldsymbol{k}\sigma\sigma'} \sigma^{0(z)}_{\sigma\sigma'} f^{\boldsymbol{q}}_{\boldsymbol{k}} c^\dagger_{\boldsymbol{k}+\boldsymbol{q}\sigma}(\tau) c_{\boldsymbol{k}\sigma'}(\tau), \tag{3}$$

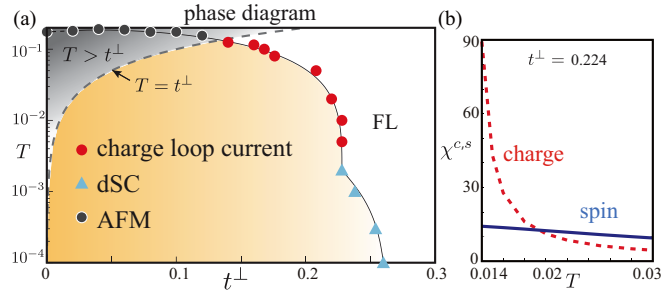

FIG. 3. (a) Obtained phase diagram. The cLC appears in the FL regime. (b) Temperature dependence of the susceptibilities for the charge-ch (dotted line) and spin-ch (solid line).

where τ is imaginary time. $\hat{\sigma}^0$ is the identity matrix and $\hat{\sigma}^z$ is the Pauli matrix. Here, we optimize the form factor $f_{\boldsymbol{k}}^{\boldsymbol{q}}$ unbiasedly to maximize $\chi^c(\boldsymbol{q})$ at each $\boldsymbol{q}$ point using the Lagrange multiplier method; see SM A [60].

The form factor corresponds to the modulation of the correlated hopping integral from j to the i site, δt_{ij} ($i \neq j$). It is given as $\delta t_{ij} = \Delta t \sum_k f_k^{\boldsymbol{q}=\boldsymbol{0}} e^{ik(r_i - r_j)}$ for the uniform modulation. Here, both the bond order ($\delta t_{ij} = \delta t_{ji}$) and the cLC ($\delta t_{ij} = -\delta t_{ji}$) are described. Due to the Hermite condition, δt_{ij} for the cLC order is purely imaginary. In Figs. 2(d) and 2(e), we plot the $\boldsymbol{q}$ dependence of the charge- and spin-ch susceptibilities, respectively. The strong charge-ch fluctuations develop at $\boldsymbol{q} = \boldsymbol{0}$, while the spin fluctuations remain small even at the peak $\boldsymbol{q} = (\pi, \pi/2) \equiv \boldsymbol{Q}_{\rm AFM}$. Figure 2(f) shows the charge-ch form factor at $\boldsymbol{q} = \boldsymbol{0}$. For a fixed k_y, the relation $f_{k_x}^{\boldsymbol{0}} \simeq -f_{-k_x}^{\boldsymbol{0}}$ ($\propto \sin k_x + b \sin 3k_x$) holds. Then, the real-space order parameter is $\delta t_{ij} = -\delta t_{ji}$ that leads to the emergence of ferro-cLC order. The third-nearest-intrachain form factor derived from the present fRG is significant for realizing the cLC [60]. In Fig. 2(g), we show the schematic picture of the cLC, which is a magnetic-octupole-toroidal order. A detailed explanation of the numerical results is shown in Fig. S4 in SM B [60].

In Fig. 3(a), the obtained phase diagram in the T-$t^\perp$ space is plotted. We reveal that the cLC phase appears around $t^\perp \simeq 0.2$ as an intertwined order between the AFM and dSC states. Note that the dark shaded area is the 1D Mott insulating phase that is beyond the scope of the present study [55,56]. In addition, Fig. 3(b) shows the T dependence of the $\chi^c(\boldsymbol{0})$ and $\chi^s(\boldsymbol{Q}_{\rm AFM})$. $\chi^c(\boldsymbol{0})$ drastically develops at low temperatures. The transition temperatures in Fig. 3(a) are determined under the condition that the largest susceptibility (spin, charge, dSC) exceeds $\chi_{\rm max} = 30$, while the phase diagram is insensitive to $\chi_{\rm max}$ ($\gg$10), as recognized in Fig. 3(b). As a result, the cLC phase is stabilized in the FL region around $t_\perp \gg T$.

To understand the origin of the cLC, we analyze the charge (spin)-ch four-point vertex function defined by

$$g_{pp'}^{c(s)}(\boldsymbol{q}) \equiv g_{p\uparrow p+q\uparrow p'\uparrow p'+q\uparrow} + (-) g_{p\uparrow p+q\uparrow p'\downarrow p'+q\downarrow}. \tag{4}$$

In Fig. 4(a), we plot the patch dependence of the charge-ch four-point vertex $g_{pp'}^c(\boldsymbol{0})$. The relation $g_{\boldsymbol{RR'}}^c(\boldsymbol{0}) \approx -g_{\boldsymbol{LR}}^c(\boldsymbol{0})$ holds, where $\boldsymbol{R} = 1$–24 ($\boldsymbol{L} = 25$–48) is the patch index in the right (left) branch. We also plot the flow (l dependence) of the four-point vertex in Fig. 4(b). $g_{\boldsymbol{RR'}}^c(\boldsymbol{0})$ comes to be a large negative value, while $g_{\boldsymbol{LR}}^c(\boldsymbol{0})$ takes a large positive value.

In order to explain why the odd-parity form factor is obtained, we introduce $\bar{g}_{RR}^{c(s)}(\boldsymbol{q})$, $\bar{g}_{LR}^{c(s)}(\boldsymbol{q})$, $\bar{f}_R^{\boldsymbol{0}}$, $\bar{f}_L^{\boldsymbol{0}}$ as their maximum values in the patch space. In this case, the charge-ch susceptibility is

$$\chi^c(\boldsymbol{0}) \propto -\left(\bar{f}_R^{\boldsymbol{0}}\right)^2 \bar{g}_{RR}^c(\boldsymbol{0}) - \bar{f}_L^{\boldsymbol{0}} \bar{f}_R^{\boldsymbol{0}} \bar{g}_{LR}^c(\boldsymbol{0}), \tag{5}$$

as shown in Fig. 2(c). Since $\bar{g}_{RR}^c(\boldsymbol{0})$ is negative and $\bar{g}_{LR}^c(\boldsymbol{0})$ is positive, the relation $\bar{f}_R^{\boldsymbol{0}} = -\bar{f}_L^{\boldsymbol{0}}$ is required to maximize the susceptibility. In conclusion, the odd-parity cLC appears due to the sign reversal between $\bar{g}_{RR}^c(\boldsymbol{0})$ and $\bar{g}_{LR}^c(\boldsymbol{0})$ in the FL region. As for the spin-ch susceptibilities, both $g_{RR}^s(\boldsymbol{Q}_{\rm AFM})$ and $g_{LR}^s(\boldsymbol{Q}_{\rm AFM})$ are negative, and therefore the spin-ch form factor does not have any sign reversal on the FS as shown in

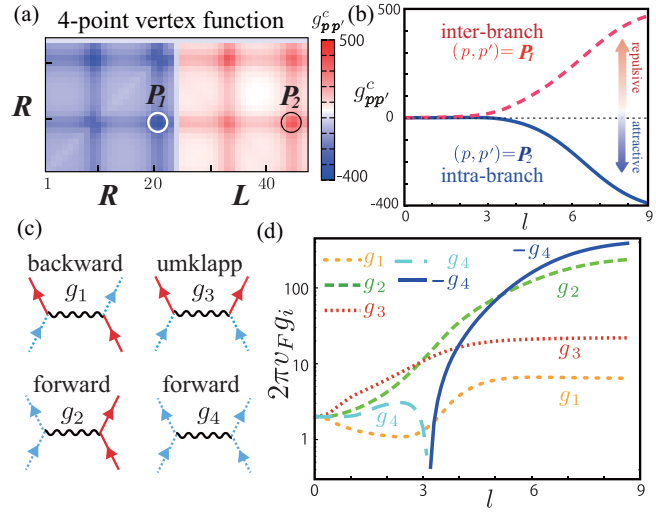

FIG. 4. (a) Patch dependence of four-point vertex at $\boldsymbol{q} = \boldsymbol{0}$. The obtained relation $g_{\boldsymbol{RR}}^c(\boldsymbol{0}) \approx -g_{\boldsymbol{LR}}^c(\boldsymbol{0})$ gives the ferro-cLC. (b) Flow of $g_{pp'}^c(\boldsymbol{0})$. $g_{\boldsymbol{RR(LR)}}^c(\boldsymbol{0})$ takes a large negative (positive) value as the cutoff energy decreases. (c) Definition of the g_i in the g-ology theory. The dotted (solid) line gives an electron on the right (left) branch. (d) Obtained flow of g_i.

Fig. S3 in SM A [60]. Thus, an ordinal AFM phase is realized in the 1D regime.

Here, we discuss the present result in terms of the 1D g-ology theory [54], in which the four-point vertex function is classified into four types: backward (g_1), forward (g_2, g_4), and umklapp (g_3) scatterings as defined in Fig. 4(c). As an approximation, there is a one-to-one correspondence between $\bar{g}_{pp'}^{c(s)}(\boldsymbol{q})$ and g_i ($i = 1$–4) as

$$\begin{aligned} &\bar{g}_{RR}^c(\boldsymbol{0}) \approx 2\pi v_F g_4, \quad \bar{g}_{LR}^c(\boldsymbol{0}) \approx 2\pi v_F (2g_2 - g_1), \\ &\bar{g}_{RR}^s(\boldsymbol{Q}_{\rm AFM}) \approx -2\pi v_F g_2, \quad \bar{g}_{LR}^s(\boldsymbol{Q}_{\rm AFM}) \approx -2\pi v_F g_3, \end{aligned} \tag{6}$$

where v_F is the Fermi velocity.

Based on Eq. (6), we plot the flow of g_i in Fig. 4(d). We find that g_4 (g_2) has a large negative (positive) value as the l increases. The present result is understood by using the knowledge of the g-ology theory as we discuss in SM D [60]: At half filling, g_2 is relevant due to the Peierls-ch scattering [54]. In the present Q1D model, the frustrated hopping $t^\perp$ violates the perfect nesting condition, and therefore g_2 (or AFM fluctuation) is relatively suppressed at $\Lambda_l < t^\perp$ compared with pure 1D systems [53–58]. On the other hand, surprisingly, g_4 takes large negative values due to the Landau-ch scattering that is important at low energies ($\Lambda_l < T$). As a result, 1D AFM instability is suppressed by $t^\perp$, and the cLC due to the Landau-ch instead appears. [The importance of g_4 on $\chi^s(\boldsymbol{0})$ was discussed in Ref. [61].] Thus, the geometrical frustration is essential for realizing the cLC order.

Also, the cLC is naturally understood by the spin-fluctuation-driven mechanism based on the 2D FL concept [62–64]. To show this, we solve the "particle-hole (ph) gap

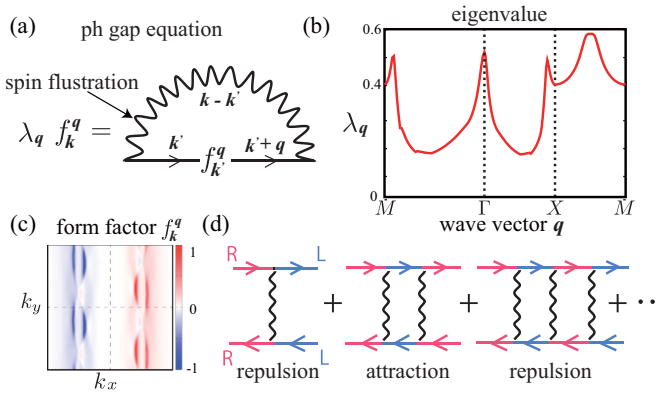

FIG. 5. (a) The ph gap equation. The wavy line is the spin fluctuations given by the RPA. (b) Obtained eigenvalue of the gap equation at $(T, U) = (0.03, 1.65)$. The peak around the Γ point corresponds to the cLC. (c) Obtained charge-ch form factor at $\boldsymbol{q} = \boldsymbol{0}$, which is essentially the same as the fRG results. (d) Dominant contribution for stabilizing the cLC order.

equation" for the charge-ch form factor $f_{\boldsymbol{k}}^{\boldsymbol{q}}$,

$$\lambda_{\boldsymbol{q}} f_{\boldsymbol{k}}^{\boldsymbol{q}} = \sum_{\boldsymbol{k}'} f_{\boldsymbol{k}'}^{\boldsymbol{q}} L(\boldsymbol{k}', \boldsymbol{q}) \left(-\frac{3}{2} V^s_{\boldsymbol{k}-\boldsymbol{k}'} - \frac{1}{2} V^c_{\boldsymbol{k}-\boldsymbol{k}'} \right), \tag{7}$$

where $\lambda_{\boldsymbol{q}}$ is the eigenvalue. Here, we define $V_{\boldsymbol{q}}^{c(s)} \equiv -(+)U + U^2 \chi^{c(s)}(\boldsymbol{q})$ in the random-phase approximation (RPA), and $L(\boldsymbol{k}, \boldsymbol{q}) \equiv (n_{\boldsymbol{k}-\frac{\boldsymbol{q}}{2}} - n_{\boldsymbol{k}+\frac{\boldsymbol{q}}{2}})/(\epsilon_{\boldsymbol{k}+\frac{\boldsymbol{q}}{2}} - \epsilon_{\boldsymbol{k}-\frac{\boldsymbol{q}}{2}}) > 0$ with the Fermi distribution function $n_{\boldsymbol{k}}$. The diagrammatic expression of the ph gap equation in Fig. 5(a) is given by the first-order spin-fluctuation exchange term (= Maki-Thompson (MT)-type process). Figure 5(b) shows the largest eigenvalue $\lambda_{\boldsymbol{q}}$ for general $\boldsymbol{q}$. The second largest peak at the Γ point corresponds to the cLC since the obtained odd-parity form factor in Fig. 5(c) is essentially the same as the results by the fRG. (Obviously, the fRG method is superior to RPA in that loop cancellation in 1D system is taken into account.) Figure 5(d) shows the scattering processes generated by solving the ph gap equation. The even (odd)-order processes with respect to $\chi^s(\boldsymbol{Q}_{\rm AFM})$ work as interbranch repulsion (intrabranch attraction), which corresponds to $\bar{g}^c_{RR} < 0$ ($\bar{g}^c_{LR} > 0$) in Fig. 4(a). Thus, the cLC is naturally explained in terms of the FL concept, and this mechanism is found to be similar to that for the dSC near the AFM phase [55–58,65].

Furthermore, we perform the fRG without Cooper-ch processes and confirm that the cLC is obtained even if we neglect the Cooper-ch as shown in Fig. S5 in SM C [60]. Thus, we conclude that the cLC emerges due to the spin-fluctuation-driven mechanism.

Next, we discuss the dSC phase. Figure 6(a) shows the optimized SC gap given by the fRG [15]. This dSC gap is well understood in terms of the singlet SC gap equation with the MT process [65],

$$\lambda^{\rm SC} \Delta_{\boldsymbol{k}} = \sum_{\boldsymbol{k}'} \Delta_{\boldsymbol{k}'} C(\boldsymbol{k}') \left(-\frac{3}{2} V^s_{\boldsymbol{k}-\boldsymbol{k}'} + \frac{1}{2} V^c_{\boldsymbol{k}-\boldsymbol{k}'} \right), \tag{8}$$

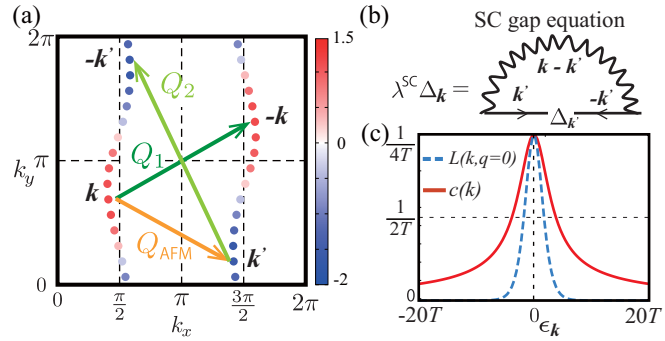

FIG. 6. (a) dSC gap function obtained by the fRG. (b) SC gap equation. (c) $\epsilon_{\boldsymbol{k}}$ dependence of $L(\boldsymbol{k}, \boldsymbol{q} = 0)$ and $C(\boldsymbol{k})$.

where $C(\boldsymbol{k}) = (2n_{\boldsymbol{k}} - 1)/(2\epsilon_{\boldsymbol{k}}) > 0$ and its diagrammatic expression is in Fig. 6(b). Since $\Delta_{\boldsymbol{k}}$ is even parity, the interbranch repulsion by $V^s_{\boldsymbol{Q}_{\rm AFM}}$ induces the nodal dSC.

Furthermore, we discuss the reason why the cLC phase dominates over the SC phase. As shown in Fig. 6(c), $C(\boldsymbol{k})$ in Eq. (8) is always larger than $L(\boldsymbol{k}, \boldsymbol{q} = \boldsymbol{0})$ in Eq. (7) except at $\epsilon_{\boldsymbol{k}} = 0$, reflecting the logarithmic Cooper-ch singularity [54]. On the other hand, the Cooper instability is reduced by the intrabranch sign reversal in the dSC gap. By considering the dominant contribution of the gap function at $(\boldsymbol{k}, \boldsymbol{k}', -\boldsymbol{k}, -\boldsymbol{k}')$ in Fig. 6(a), the effective pairing interaction for the d-wave gap is

$$V_{d\rm SC} \propto \{2\chi^s(\boldsymbol{Q}_{\rm AFM}) - \chi^s(\boldsymbol{Q}_1) - \chi^s(\boldsymbol{Q}_2)\} \propto (t^\perp/t)^2. \tag{9}$$

Thus, the d-wave Cooper instability is suppressed by the factor $(t^\perp/t)^2 \ll 1$ due to the 1D nature.

If we consider an off-site Coulomb interaction V in addition to U, the cLC instability should be enhanced. In fact, the Fock term $-2V\cos(\boldsymbol{k} - \boldsymbol{k}')$ is added to $V^c_{\boldsymbol{k}-\boldsymbol{k}'}$ in Eq. (7), and it gives the interbranch repulsive and intrabranch attractive interactions [20,22,23,25]. Thus, both the spin fluctuation and finite off-site Coulomb V will cooperatively stabilize the cLC phase.

In summary, we proposed the spin-fluctuation-driven cLC mechanism based on the fRG theory. We derived the optimized form factor, which is the key essence of the unconventional order, without any assumptions. By virtue of this method, the ferro-cLC order is obtained without any bias in a simple frustrated chain Hubbard model. For the microscopic origin of the cLC, the strong renormalization of the forward scatterings (g_2, g_4) due to spin fluctuations plays an important role. We stress that the cLC phase in the FL regions is replaced with the AFM phase if we remove the frustration as shown in Fig. S9 in SM E. The role of geometrical frustration is to realize strong short-range spin fluctuations that mediate the cLC order. Thus, it will be useful to verify the theoretically predicted correlation between the cLC order and spin fluctuation strength in future experiments.

We are grateful to S. Onari and M. Tsuchiizu for useful discussions. This work is supported by Grants-in-Aid for Scientific Research (KAKENHI) Research (No. JP20K22328, No. JP20K03858, No. JP19H05825, and No. JP18H01175) from MEXT of Japan.

[1] R. M. Fernandes, L. H. VanBebber, S. Bhattacharya, P. Chandra, V. Keppens, D. Mandrus, M. A. McGuire, B. C. Sales, A. S. Sefat, and J. Schmalian, Phys. Rev. Lett. **105**, 157003 (2010).

[2] R. M. Fernandes, A. V. Chubukov, J. Knolle, I. Eremin, and J. Schmalian, Phys. Rev. B **85**, 024534 (2012)

[3] A. V. Chubukov, M. Khodas, and R. M. Fernandes, Phys. Rev. X **6**, 041045 (2016).

[4] R.-Q. Xing, L. Classen, and A. V. Chubukov, Phys. Rev. B **98**, 041108(R) (2018).

[5] S. Onari and H. Kontani, Phys. Rev. Lett. **109**, 137001 (2012).

[6] S. Onari, Y. Yamakawa, and H. Kontani, Phys. Rev. Lett. **116**, 227001 (2016).

[7] Y. Yamakawa, S. Onari, and H. Kontani, Phys. Rev. X **6**, 021032 (2016).

[8] H. J. Schulz, Phys. Rev. B **39**, 2940(R) (1989).

[9] M. A. Metlitski and S. Sachdev, New J. Phys. **12**, 105007 (2010).

[10] S. Sachdev and R. La Placa, Phys. Rev. Lett. **111**, 027202 (2013).

[11] J. C. S. Davis and D.-H. Lee, Proc. Natl. Acad. Sci. U.S.A. **110**, 17623 (2013).

[12] E. Berg, E. Fradkin, S. A. Kivelson, and J. M. Tranquada, New J. Phys. **11**, 115004 (2009).

[13] Y. Yamakawa and H. Kontani, Phys. Rev. Lett. **114**, 257001 (2015).

[14] K. Kawaguchi, Y. Yamakawa, M. Tsuchiizu, and H. Kontani, J. Phys. Soc. Jpn. **86**, 063707 (2017).

[15] M. Tsuchiizu, Y. Yamakawa, and H. Kontani, Phys. Rev. B **93**, 155148 (2016).

[16] M. Tsuchiizu, K. Kawaguchi, Y. Yamakawa, and H. Kontani, Phys. Rev. B **97**, 165131 (2018).

[17] Y. Wang and A. V. Chubukov, Phys. Rev. B **90**, 035149 (2014).

[18] H. Ikeda, M.-T. Suzuki, R. Arita, T. Takimoto, T. Shibauchi, and Y. Matsuda, Nat. Phys. **8**, 528 (2012).

[19] R. Tazai and H. Kontani, Phys. Rev. B **100**, 241103(R) (2019).

[20] A. A. Nersesyan, G. I. Japaridze, and I. G. Kimeridze, J. Phys.: Condens. Matter **3**, 3353 (1991).

[21] H. Kontani, Y. Yamakawa, R. Tazai, and S. Onari, Phys. Rev. Research **3**, 013127 (2021).

[22] C. M. Varma, Phys. Rev. B **55**, 14554 (1997).

[23] C. Weber, T. Giamarchi, and C. M. Varma, Phys. Rev. Lett. **112**, 117001 (2014).

[24] I. Affleck and J. B. Marston, Phys. Rev. B **37**, 3774(R) (1988).

[25] S. Bulut, A. P. Kampf, and W. A. Atkinson, Phys. Rev. B **92**, 195140 (2015).

[26] H. Yokoyama, S. Tamura, and M. Ogata, J. Phys. Soc. Jpn. **85**, 124707 (2016).

[27] T. K. Lee and L. N. Chang, Phys. Rev. B **42**, 8720 (1990).

[28] M. Ogata, B. Doucot, and T. M. Rice, Phys. Rev. B **43**, 5582 (1991).

[29] F. C. Zhang, Phys. Rev. Lett. **64**, 974 (1990).

[30] P. Chudzinski, M. Gabay, and T. Giamarchi, Phys. Rev. B **78**, 075124 (2008).

[31] S. Chatterjee, S. Sachdev, and M. S. Scheurer, Phys. Rev. Lett. **119**, 227002 (2017).

[32] M. S. Scheurer and S. Sachdev, Phys. Rev. B **98**, 235126 (2018).

[33] J. O. Fjærestad, J. B. Marston, and U. Schollwöck, Ann. Phys. **321**, 894 (2006).

[34] M. Tsuchiizu and A. Furusaki, Phys. Rev. B **66**, 245106 (2002).

[35] D. Bounoua, L. Mangin-Thro, J. Jeong, R. Saint-Martin, L. Pinsard-Gaudart, Y. Sidis, and P. Bourges, Commun. Phys. **3**, 123 (2020).

[36] L. Mangin-Thro, Y. Sidis, A. Wildes, and P. Bourges, Nat. Commun. **6**, 7705 (2015).

[37] L. Mangin-Thro, Y. Sidis, P. Bourges, S. De Almeida-Didry, F. Giovannelli, and I. Laffez-Monot, Phys. Rev. B **89**, 094523 (2014).

[38] J. Jeong, Y. Sidis, A. Louat, V. Brouet, and P. Bourges, Nat. Commun. **8**, 15119 (2017).

[39] L. Zhao, C. A. Belvin, R. Liang, D. A. Bonn, W. N. Hardy, N. P. Armitage, and D. Hsieh, Nat. Phys. **13**, 250 (2017).

[40] L. Zhao, D. H. Torchinsky, H. Chu, V. Ivanov, R. Lifshitz, R. Flint, T. Qi, G. Cao, and D. Hsieh, Nat. Phys. **12**, 32 (2016).

[41] V. M. Yakovenko, Physica B: Condens. Matter **460**, 159 (2015).

[42] H. Murayama, K. Ishida, R. Kurihara, T. Ono, Y. Sato, Y. Kasahara, H. Watanabe, Y. Yanase, G. Cao, Y. Mizukami, T. Shibauchi, Y. Matsuda, and S. Kasahara, Phys. Rev. X **11**, 011021 (2021).

[43] W. Metzner, M. Salmhofer, C. Honerkamp, V. Meden, and K. Schönhammer, Rev. Mod. Phys. **84**, 299 (2012).

[44] C. Husemann and W. Metzner, Phys. Rev. B **86**, 085113 (2012).

[45] T. Holder and W. Metzner, Phys. Rev. B **85**, 165130 (2012).

[46] M. Salmhofer and C. Honerkamp, Prog. Theor. Phys. **105**, 1 (2001).

[47] C. Honerkamp and M. Salmhofer, Phys. Rev. B **64**, 184516 (2001).

[48] C. Honerkamp, Phys. Rev. B **72**, 115103 (2005).

[49] M. Tsuchiizu, Y. Ohno, S. Onari, and H. Kontani, Phys. Rev. Lett. **111**, 057003 (2013).

[50] M. Tsuchiizu, Y. Yamakawa, S. Onari, Y. Ohno, and H. Kontani, Phys. Rev. B **91**, 155103 (2015).

[51] R. Tazai, Y. Yamakawa, M. Tsuchiizu, and H. Kontani, Phys. Rev. B **94**, 115155 (2016).

[52] P. Kopietz, L. Bartosch, and F. Schütz, *Introduction to the Functional Renormalization Group*, Lecture Notes in Physics Vol. 798 (Springer, Berlin, 2010).

[53] V. J. Emery, R. Bruinsma, and S. Barisic, Phys. Rev. Lett. **48**, 1039 (1982).

[54] C. Bourbonnais and L. G. Caron, Int. J. Mod. Phys. B **5**, 1033 (1991).

[55] J. Kishine and K. Yonemitsu, J. Phys. Soc. Jpn. **67**, 2590 (1998).

[56] J. Kishine and K. Yonemitsu, Int. J. Mod. Phys. B **16**, 711 (2002).

[57] M. Tsuchiizu and Y. Suzumura, Phys. Rev. B **59**, 12326 (1999).

[58] K. Kajiwara, M. Tsuchiizu and Y. Suzumura, and C. Bourbonnais, J. Phys. Soc. Jpn. **78**, 104702 (2009).

[59] J. Solyom, Adv. Phys. **28**, 201 (1979).

[60] See Supplemental Material at http://link.aps.org/supplemental/10.1103/PhysRevB.103.L161112 for the explanation of fRG scheme, numerical results for the cLC, numerical results

without Cooper-channel scatterings, the *g*-ology analysis, and the importance of the geometrical frustration.

[61] Y. Fuseya, M. Tsuchiizu, Y. Suzumura, and C. Bourbonnais, J. Phys. Soc. Jpn. **76**, 014709 (2007).

[62] H. Kontani, Rep. Prog. Phys. **71**, 026501 (2008).

[63] T. Moriya and K. Ueda, Adv. Phys. **49**, 555 (2000).

[64] K. Yamada, *Electron Correlation in Metals* (Cambridge University Press, Cambridge, U.K., 2004)

[65] H. Kino and H. Kontani, J. Phys. Soc. Jpn. **68**, 1481 (1999).